

Fringe fields in nonlinear photoemission microscopy

L. I. Chelaru,* M. Horn-von Hoegen, D. Thien, and F.-J. Meyer zu Heringdorf

Fachbereich Physik, Universität Duisburg-Essen (Campus Duisburg), 47057 Duisburg, Germany

(Received 24 June 2005; revised manuscript received 12 January 2006; published 16 March 2006)

Self-organized Ag nanostructures have been investigated by photoemission electron microscopy where the electrons are generated by femtosecond laser pulses through a two-photon photoemission process. Bright and dark areas are observed around the nanostructures when they exceed a certain lateral dimension. The features are different for both directions of the polarization of the incoming light and s and p polarization. In p polarization the features consist of several interference fringes that are explained by diffraction. The photoemission yield of Ag nanowires also shows a dependence on the polarization direction of the incoming light with respect to the orientation of the nanowire. This is explained with a particle plasmon state in the Ag nanostructures that acts as the intermediate state for two-photon photoemission. Also, we present evidence of far-field mediating interaction between neighboring Ag nanostructures.

DOI: [10.1103/PhysRevB.73.115416](https://doi.org/10.1103/PhysRevB.73.115416)

PACS number(s): 68.37.-d, 73.20.Mf

I. INTRODUCTION

Trapping of light in nanostructures, the guiding of light as plasmon-polariton waves inside a metallic layer, local field enhancement around metal nanoparticles, and novel photonic band gap materials offer exciting possibilities for future nano-optics-based device applications.¹ Most of the new and proposed devices make use of the local scattering processes of light in and around small structures. To analyze the scattered light, one would require either numerical methods or rather cumbersome and difficult to interpret experiments like scanning near-field optical microscopy (SNOM) or photon scanning tunneling microscopy (PSTM).² We show that two-photon photoemission microscopy (2PPEEM) is well suited to analyze the interaction of light with metallic particles on a surface.

Illumination of a sample surface with photons of an energy larger than the photoelectric work function leads to the emission of photoelectrons. In photoelectron emission microscopy (PEEM), this is usually achieved by using ultraviolet light from a mercury discharge lamp or synchrotron radiation. The photoemission yield (i.e., the total number of photoemitted electrons) varies locally over the surface, since it depends on the local electronic and morphologic structure. Islands of a material with a lower work function, for instance, would have a higher photoelectron yield. PEEM uses the local differences in the photoemission yield to generate an image. If a laser is used for illumination, however, the energy of the laser light is typically lower than the photoelectric work function of the surface and usually no electrons are emitted. Only if the laser intensity is sufficiently high can nonlinear emission processes trigger higher-order emission. A photoemission process that needs n photons is commonly referred to as n -photon photoemission (nPPE). While classic photoemission³ predicts a linear dependence of the photoemission yield (Y) with light intensity (I), the usual picture for n photon photoemission assumes that n photons simultaneously excite one electron from the Fermi level into the vacuum, which yields⁴ $Y_{nPPE} \propto I^n$. The necessary intensities for this can only be obtained from pulsed laser sources such

as the popular mode-locked Ti:sapphire laser oscillators. The strong nonlinear dependence of the 2PPE photoemission yield Y on the electric field intensity makes two-photon photoemission microscopy highly sensitive to small variations of the exciting field and recommends it as a technique for the investigation of light interactions with metal surfaces.

II. EXPERIMENT

We used the spectroscopic photoelectron emission microscope (ELMITEC PEEM III) with imaging energy analyzer⁵ located at the University of Duisburg-Essen. The ultrahigh-vacuum (UHV) microscope provides a maximum lateral resolution of 11 nm. Silver islands and nanowires were grown *in situ* on 4° vicinal Si(001) substrates inside the microscope using a home built evaporation system^{6,7} following the procedure described by Roos *et al.*:⁸ During deposition, after the completion of the first (3×2) reconstructed Ag monolayer,⁹ small rectangular islands and quasi-one-dimensional nanowires are formed that exhibit a typical height and width of 150–300 nm and a variable length of tens of micrometers.

We used a commercial 800-nm fs-Ti:sapphire laser oscillator (FEMTOLASERS) with a repetition rate of 80 MHz for illumination. The 20-fs short pulses were frequency doubled in a beta barium borate (BBO) crystal with an effectivity of 14%. The resulting 400-nm (3.1 eV) pulses had a maximum pulse energy of 1 nJ. After a standard dispersion correction¹⁰ we obtain a pulse length of 40 fs in the vacuum as determined by an interferometric pump-probe autocorrelation trace. For Ag, with a photoelectric work function between 4.6 and 4.8 eV (depending on the crystallographic orientation¹¹), these pulses create a significant photoemission yield via a two-photon photoemission process.

III. RESULTS AND DISCUSSION

The order of the photoemission process can easily be verified by variation of the laser intensity and recording of the photoemission yield. Figure 1 shows the normalized photo-

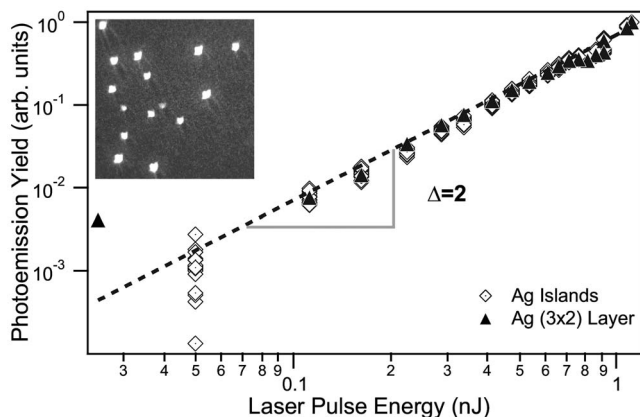


FIG. 1. Log-log plot of the photoemission yield in arbitrary units as a function of the incident laser pulse intensity. The dashed line represents a fit of the experimental data points with a power law function with exponent $\Delta=2.0$. The markers correspond to the measured photoemission yield of each individual Ag nanostructure and the background.

emission yield of various features of the surface as a function of the laser intensity in a double-logarithmic plot. Open squares represent the Ag islands from the inset; dark triangles represent the (3×2)Ag wetting layer between the islands. The fit in Fig. 1 corresponds to a power law with an exponent of $\Delta=2.0$, clearly indicating that in our case the photoemission proceeds via a 2PPE process.

A. Photoemission yield enhancement through particle plasmon excitation

We will now show that the intermediate state for 2PPE is linked to a particle plasmon in the Ag nanostructures. Although surface-plasmon-mediated photoemission enhancement has been known for a decade, the origin of this enhancement is still under debate.¹² For the Ag islands it is known that the absorption of the first photon leads to the excitation of a particle plasmon, while the absorption of a

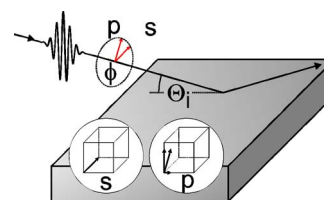


FIG. 3. (Color online) Schematic representation of the electric field component at the sample surface of the *s*- and *p*-polarized femtosecond pulses.

second photon triggers the emission of an electron.^{13,14}

Figure 2 shows PEEM images of the same area on the surface under different illumination and illustrates the 2PPE yield enhancement due to particle plasmon excitation. In (a), the sample is illuminated with a mercury discharge lamp (maximum 4.9 eV) and the image shows regular one photon photoemission contrast. The panels (b) and (c) were taken under illumination with $\lambda=400$ nm laser pulses and show the dependence of the photoemission yield on the polarization direction of the incoming light. To avoid confusion we define *s* and *p* polarization relative to our laser table (see the sketch in Fig. 3): while the electric field vector of the *s*-polarized light lies completely in the sample plane, the *p*-polarized light has a component normal to the sample surface and also a component in the surface plane caused by the grazing incidence illumination under an angle of 74° relative to the surface normal. In Fig. 2 the in-plane directions of the electric field for *p*- and *s*-polarized light are schematically shown at the left bottom side in panels (b) and (c).

The surface morphology in Fig. 2(a) is dominated by Ag islands and nanowires on top of the (3×2)Ag wetting layer. Scanning emission microscopy reveals that a typical Ag island on Si(001) has a pyramidal shape, with a height of less than 250 nm. While all Ag nanostructures appear bright on a dark background in (a), the photoemission yield of individual islands shows a strong polarization dependence under laser illumination. The long nanowire (marked by arrow “A”) appears bright in (b) when the electric field is perpendicular to its long axis and the energy of the laser light coincides well

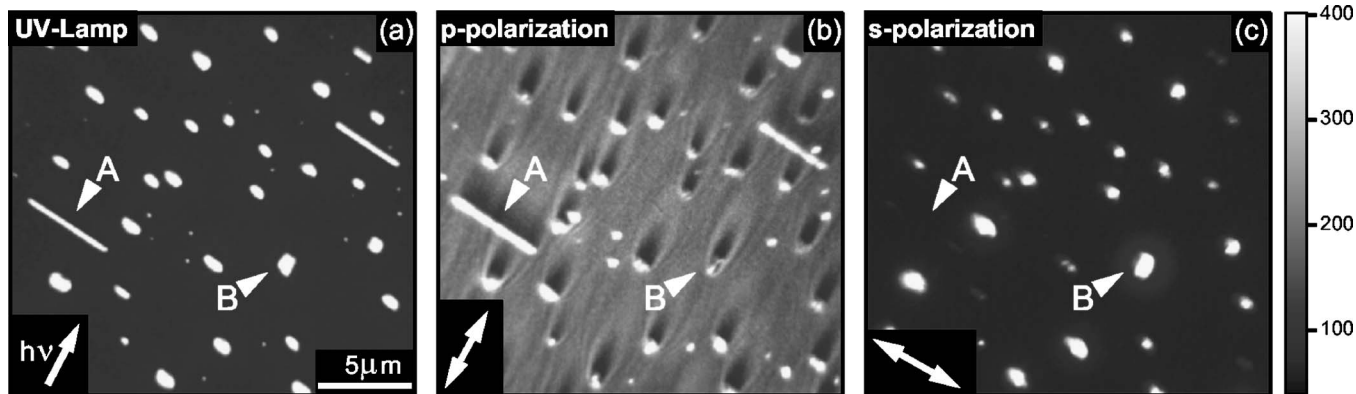


FIG. 2. PEEM images of Ag/Si(001): (a) sample illuminated by UV light (Hg discharge lamp, $h\nu \approx 4.9$ eV) and (b) and (c) same area as in panel (a) illuminated by *p*- and *s*-polarized femtosecond laser light ($h\nu=3.1$ eV). The direction of the incoming light is shown by the white arrow at the left bottom of panel (a). The arrows at the lower left in (b) and (c) indicate the direction of the in-plane component of the electric field.

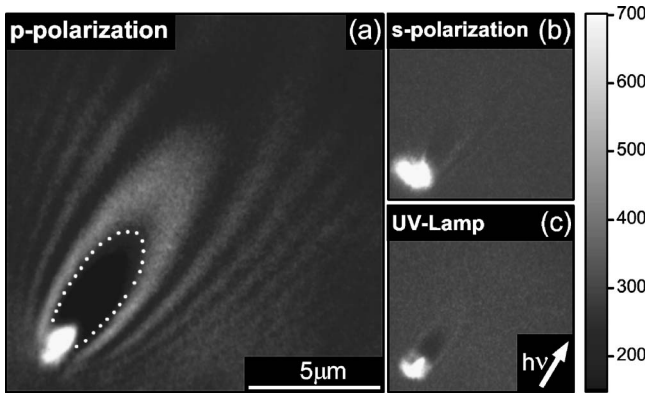


FIG. 4. Micrograph PEEM images of Ag/Si(001): (a) and (b) sample illuminated by p - and s -polarized femtosecond laser light ($h\nu=3.1$ eV) and (c) same area as in panel (a) and (b) illuminated by UV light. The white dashed line marks the position of the first diffraction maximum. The direction of the incoming light is shown by the white arrow at the right bottom of panel (c). The grayscale level in panels (b) and (c) is scaled to reveal details in the background.

with the particle plasmon resonance. The same Ag nanowire appears dark in panel (c), however, when the electric field lies parallel to the long axis of the nanowire and cannot excite the particle plasmon since the plasmon resonance frequency has shifted to lower energies¹⁵ (larger noble-metal clusters generally have lower plasmon resonances with shorter lifetimes¹⁶). The behavior is reversed for the short nanowire marked by arrow “B,” which is rotated by 90° with respect to nanowire “A.” Wire “B” also only appears bright when the electric field is perpendicular to its long axis, which is the case in panel (c). Accordingly, only the beginning and the end of the nanowires show up in panel (b). Smaller rectangular islands are visible under both polarizations.

The striking feature in Fig. 2 is that the background intensity in panel (c) is much lower than in (b), $\left(\frac{Y_s}{Y_p}\right)_{\text{expt}} \approx 0.033$, as estimated from the photoemission yield after background subtraction.

Since in our geometry, the p -polarized light has a significant component of the electrical field perpendicular to the surface that is not present in s -polarized light, we can only explain the high-yield variation by assuming that the field component perpendicular to the surface is responsible for the photoemission. We suspect one of the known Ag (3×2) surface states¹⁸ to act as the initial state for the photoemission signal in the background.

B. Observation of fringe fields

The most prominent feature in Fig. 2(b) is the dark area that lies behind the islands in the direction of the incoming light.

Figure 4 shows a single Ag island with its surrounding area under illumination with p -polarized laser pulses (a), s -polarized laser pulses (b), and under illumination with a mercury discharge lamp (c). For p -polarized light, Fig. 4(a),

a dark area and several bright and dark fringes are visible behind the Ag island. Even if the contrast and brightness in panels (b) and (c) are adjusted to reveal the slightest modulations in the background, none of the fringes are visible when the sample is illuminated with s -polarized light (b) or with the mercury discharge lamp (c).

Let us now focus our discussion on the fringe fields and the origin of the dark area behind the islands, marked by a dotted line in Fig. 4(a). The dark area cannot be explained by a simple shadowing effect. In our geometry, a shadow of a 250-nm-high island would extend only 900 nm over the surface. The dark area behind the islands, however, extends several μm over the surface.

The dark area does also not simply reflect the optical near fields. As a rule of thumb, if an aperture with diameter a is illuminated with plane waves of wavelength λ , the field distribution can only be described by Fresnel diffraction (near-field) within a distance of $R \leq \frac{a^2}{\lambda}$ behind the aperture.¹⁷ Outside R , the diffraction pattern is described by regular Fraunhofer diffraction (far-field). According to this rule, for 250-nm-large Ag islands on a surface that are illuminated with $\lambda=400$ nm light under grazing incidence, the near-field zone extends only 150 nm over the surface, followed by a stationary fringe field distribution in the far-field zone. Thus, the dark area behind the Ag islands does not reflect the near-field zone but indeed corresponds to the far-field zone.

The shape of the fringes around the island suggests that the pattern might be formed just by regular light diffraction. For the simple case of the illumination of a circular aperture with coherent plane waves, the intensity distribution is well known:

$$I \propto \left[\frac{J_1(x)}{x} \right]^2 \quad (1)$$

Here, $J_1(x)$ is a first-order Bessel function, $x = \frac{\pi}{\lambda} a \sin \theta$, with a for the diameter of the aperture, λ for the wavelength of the incoming light, and the scattering angle θ . The diffraction pattern on a screen perpendicular to the optical axis shows a central maximum where more than 90% of the diffracted light is located, followed by a series of concentric circles of maximum and minimum intensity. The maxima (minima) of the diffraction are given by the maxima (minima) of $\frac{J_1(x)}{x}$ with the first minimum at $m_0=3.83166$. From this, the radius r of the first maximum diffraction circle on a screen at the distance d can be expressed as

$$r = m_0 \frac{\lambda d}{\pi a}. \quad (2)$$

Babinet’s principle states similarity of Fraunhofer diffraction patterns of complementary objects like an aperture and an opaque object of the same shape.¹⁷ The only difference between the two cases is that the electric fields of all interfering waves are shifted by 180° . Hence, behind the Ag

nanoslands we will expect to see a Fraunhofer diffraction pattern similar to the diffraction pattern of an aperture. The diffracted light by the Ag nanoislands is distributed within a cone. This can be easily explained by our geometry. Since the probing screen—the (3×2) Ag wetting layer—is oriented under grazing incidence with respect to the direction of the incoming light, the diffraction pattern will be a cross section across the diffraction cone with an elliptical shape. The intensity directly behind the Ag nanoislands, however, is minimal. This is caused by the interference between the incident light and the scattered light, which are 180° out-of-phase due to Babinet's principle.

From Eq. (2) we can estimate the dimension of the dark area behind the Ag nanoislands as

$$r = m_0 \frac{\lambda}{\sin \alpha} \frac{h}{\pi a}, \quad (3)$$

where again $\lambda=400$ nm, $\alpha=15^\circ$, h is the height of the particle, and a is the diameter of the particle. For a 250-nm-high and 250-nm-wide particle we calculate the size of the dark area behind the particle from Eq. (3) to $3.8 \mu\text{m}$.

With this explanation, it seems astonishing that the fringe field is not observed in panel (c) of Fig. 4 under illumination with the mercury discharge lamp. The UV light of the mercury discharge lamp is not polarized and should also have a p -polarized component. The difference between (a) and (c) is that in (a) a two-photon process is necessary for photoemission, while in (c) the photoemission proceeds via a one-photon process. Based on the nature of 2PPE where $Y_{2PPE} \propto I^2$, the 2PPE signal is much more sensitive to slight variations of the electric field than regular photoemission, where simply $Y_{PPE} \propto I$. Thus, 2PPE strongly amplifies the interference fringe contrast of the scattered light around the island.

Surprisingly, the dark areas and fringe fields have so far not been observed in 2PPEEM, although other groups have already studied Ag particles deposited on ITO or SiO_2 (Refs. 19 and 20) with this technique. When Ag nanoislands are deposited on SiO_2 with a photoelectric work function of 8.4 eV,²¹ the photoemission yield of the substrate is almost zero and thus the probing signal of the near and far fields around the Ag nanoislands is nonexistent, although the field distribution will be similar. In our case the (3×2) Ag wetting monolayer with its low photoelectric work function acts as a “detector” of the near- and far-field distributions around the Ag nanoislands. The fringe fields are not only visible for Ag islands on a (3×2) Ag monolayer. So far, we observed similar patterns around obstacles on all surfaces with a sufficiently low work function. These observations draw us to the conclusion that the *sine qua non* condition to see the near and far fields in 2PPEEM is a photoemission signal from substrate or wetting layer that can be amplified by the nonlinear nature of the 2PPE process.

C. Fringe-field Interaction

We have already shown that the excitation of a particle plasmon shows a strong dependence on the particle shape

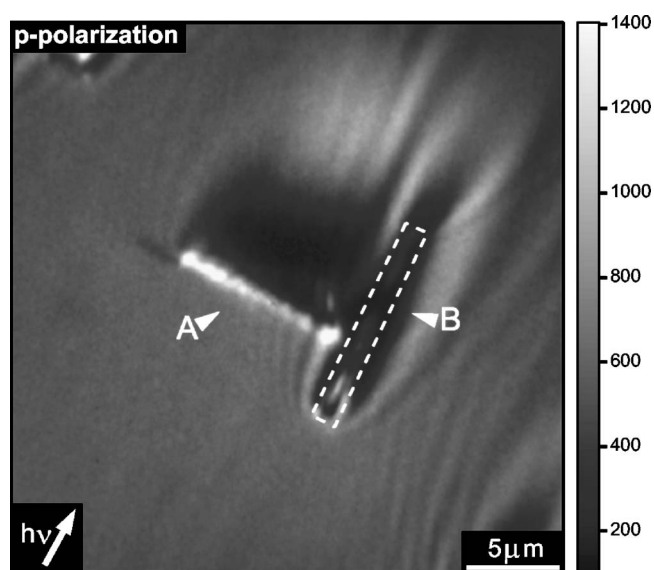


FIG. 5. 2PPEEM micrograph of two interacting Ag particles oriented along two perpendicular directions illuminated by p -polarized femtosecond pulses. The direction of the incoming light is shown by the white arrow at the left bottom side of the panel.

and that the particle modulates the electric field in its surrounding. Choosing two Ag particles in close proximity, we will now show how the far-field pattern of one wire modulates the plasmon excitation of the neighboring wire.

Figure 5 shows a 2PPEEM micrograph of two separate Ag islands labeled “A” and “B,” oriented along two perpendicular directions. The surface is illuminated with p -polarized femtosecond pulses to enhance the visibility of the fringe fields around the islands. Both Ag islands are surrounded by their respective fringe fields. The nanowire “B” appears dark based on the nonresonant excitation of the particle plasmon in the nanowire as described above and has been marked by a dotted line. An overlapping of the fringe fields of “A” and “B” is clearly visible as a modulation of the grayscale level before and behind “A.” In addition, the photoemission yield of the edge of “A” shows a variation, as a periodic change of the grayscale level, which correlates with the fringe field of the nanowire “B.” The right side of the wire “A” is located on the first maximum of the fringe field of nanowire “B” and shows a bright contrast followed by a minimum (a dark area) located on a local minimum of the fringe field of wire “B.” These minima and maxima become less pronounced as we approach the left side of “A,” reflecting the weaker modulation of the fringe fields as we move away from the nanowire “B.” The fringes visible at the lower right of the image reflect the presence of an Ag island located outside the field of view.

IV. CONCLUSIONS

In summary we have shown that a photoelectron emission microscope combined with a femtosecond laser source is a suitable technique for *in situ* investigation of light interactions with metallic particles on surfaces. The nonlinear dependence of the photoemission yield on the local field com-

ponents makes the technique very sensitive for investigations of light scattering and local field enhancement at metal surfaces. 2PPEEM opens new and promising perspectives for experimentalists from the photonics community. Excitation of particle plasmons and their dependence on the shape and size of the particles can be monitored *in situ*, during growth, while the particle dimensions can be estimated from the fringe-field pattern.

ACKNOWLEDGMENTS

The authors are thankful to P. Zhou and O. Heinz for assistance with the laser system and P. Kury for helpful discussions. Financial support from the Deutsche Forschungsgemeinschaft through SFB616 “Energy Dissipation at Surfaces” is gratefully acknowledged.

*Electronic address: liviu.chelaru@uni-due.de

- ¹W. Barnes, A. Dereux, and T. Ebbesen, *Nature (London)* **424**, 824 (2003).
²J.-J. Greffet and R. Carminati, *Prog. Surf. Sci.* **56**, 133 (1997).
³A. Einstein, *Ann. Phys. (Leipzig)* **17**, 132 (1905).
⁴M. Aeschlimann, C. A. Schmittenmaer, H. E. Elsayed-Ali, R. J. D. Miller, J. Cao, Y. Gao, and D. A. Mantell, *J. Chem. Phys.* **102**, 8606 (1995).
⁵Th. Schmidt, S. Heun, J. Slezak, J. Diaz, K. C. Prince, G. Lilienkamp, and E. Bauer, *Surf. Rev. Lett.* **5**, 1287 (1998).
⁶P. Kury, R. Hild, D. Thien, H.-L. Günter, F.-J. Meyer zu Heringdorf, and M. Horn-von Hoegen, *Rev. Sci. Instrum.* **76**, 083906 (2005).
⁷F.-J. Meyer zu Heringdorf and A. C. Belton, *Rev. Sci. Instrum.* **75**, 5288 (2004).
⁸K. R. Roos, K. L. Roos, M. Horn-von Hoegen, and F.-J. Meyer zu Heringdorf, *J. Phys.: Condens. Matter* **17**, 1407 (2005).
⁹V. Lifshits, A. Saranin, and A. Zotov, *Surface Phases on Silicon: Preparation, Structures, and Properties* (Wiley, New York, 1994).

- ¹⁰J. D. Kafka and T. Baer, *Opt. Lett.* **12**, 401 (1987).
¹¹H. B. Michaelson, *J. Appl. Phys.* **48**, 4729 (1977).
¹²M. Merschdorf, W. Pfeiffer, A. Thon, S. Voll, and G. Gerber, *Appl. Phys. A: Mater. Sci. Process.* **71**, 547 (2000).
¹³T. Tsang, T. Srinivasan-Rao, and J. Fischer, *Phys. Rev. B* **43**, 8870 (1991).
¹⁴V. M. Shalaev, C. Douketis, T. Haslett, T. Stuckless, and M. Moskovits, *Phys. Rev. B* **53**, 11193 (1996).
¹⁵C. Bohren and D. Huffman, *Absorption and Scattering of Light by Small Particles* (Wiley, New York, 1983).
¹⁶C. Sönnichsen, T. Franzl, T. Wilk, G. von Plessen, and J. Feldmann, *New J. Phys.* **4**, 93 (2002).
¹⁷E. Hecht, *Optik*, 3rd ed. (Oldenbourg, München, 2001).
¹⁸H. W. Yeom, I. Matsuda, K. Tono, and T. Ohta, *Phys. Rev. B* **57**, 3949 (1998).
¹⁹M. Cinchetti, Ph.D. dissertation, Universität Mainz, 2004.
²⁰M. Cinchetti and G. Schönhense, *J. Phys.: Condens. Matter* **17**, S1319 (2005).
²¹S. Sayan, E. Garfunkel, and S. Suzer, *Appl. Phys. Lett.* **80**, 2135 (2002).